Triaxial dynamics in the quadrupole-deformed rotor *

Qiu-Yue Li(李秋月) Xiao-Xiang Wang(王晓霞) Yan Zuo(左岩) Yu Zhang(张宇)[1)] Feng Pan(潘峰)
Department of Physics, Liaoning Normal University, Dalian 116029, China

Abstract: The triaxial dynamics of the quadrupole-deformed rotor model of both the rigid and the irrotational type are investigated in detail. The results indicate that level patterns of the two types of model can be matched with each other to the leading order of the deformation parameter β. In particular, it is found that the dynamical structure of the irrotational type with most triaxial deformation ($\gamma=30^\circ$) is equivalent to that of the rigid type with oblate deformation ($\gamma=60^\circ$), and the associated spectrum can be classified into the standard rotational bands obeying the rotational $L(L+1)$-law or regrouped into a new ground- and γ-band with odd–even staggering in the new γ-band, commonly recognized as a signature of the triaxiality. The differences between the two types of the model in this case are emphasized, especially in the E2 transitional characteristics.

Keywords: quadrupole-deformed rotor, moment of inertia, triaxial dynamics

PACS: 21.60.Ev, 21.60.Fw, 21.10.Re **DOI:** 10.1088/1674-1137/40/1/014101

1 Introduction

The quantum rotor has been widely applied to explain rotational excitations in molecules and nuclei [1–4]. For heavy or medium mass nuclei, it is often assumed that there is a quadrupole-deformed surface of these ellipsoidal nuclei [5–7], and then rotational excitations in these nuclei can be described by rotational dynamics of an ellipsoid with quadrupole deformation.

Although the quantum rotor is illustrated in many textbooks [5, 6], a detailed comparison of rotational dynamics of different types of quadrupole-deformed rotor [7] is still absent. This is an omission which should be addressed, especially when the triaxial rotor [4], which has been widely used as a basic and simple description of nuclear collectivity, has been realized microscopically within the $SU(3)$ shell model [8–10] and algebraically in the interacting boson model [11–13]. Particularly, our recent analysis [13] shows that the E2 properties in the $SU(3)$ image of the quadrupole-deformed rotor are closer to those obtained from the rigid type rotor. On the other hand, the values of moments of inertia extracted from experiments may approach those obtained from the irrotational type rotor. The dynamical differences between the two types of rotor in an axial-deformed case is well known [5–7]. However, the situations in the triaxial-deformed case remain to be investigated. More recently, a triaxial rotor model with independent inertia and E2 tensors was suggested [14–17], which provides new insights into the physics of triaxial rotations. As the triaxial rotation is explicitly defined in the quadrupole-deformed rotor, it is necessary to clarify the differences between the triaxial dynamics generated by the different types of quadrupole-deformed rotor Hamiltonian, especially by seeing that both the rigid and irrotational type rotor are used to describe nuclear collectivity [13, 18]. In this work, we will present a systematic analysis of the similarities and differences of level patterns and E2 transitional characteristics of the irrotational type model and those of the rigid type model.

2 Quadrupole-deformed ellipsoids and their moments of inertia

If only quadrupole-deformation is considered, the nuclear surface in the body-fixed frame (the principal axis system) may be described as [5, 6].

$$R(\theta,\phi)=R_0\left[1+\sum_\nu a_\nu Y_{2\nu}(\theta,\phi)\right], \tag{1}$$

where R_0 is the radius of the nucleus with spherical shape, $\{a_\nu\}$ represent components of the quadrupole deformation with

$$a_1=a_{-1}=0, \quad a_2=a_{-2}, \tag{2}$$

and $Y_{2\nu}(\theta,\phi)$ is the spherical harmonics. It is more convenient to use another set of parameters [5, 6] introduced

Received 22 April 2015
∗ Supported by National Natural Science Foundation of China (11375005, 11005056, 11175078)
1) E-mail: dlzhangyu_physics@163.com

by A. Bohr, defined by

$$\begin{aligned} a_0 &= \beta\cos\gamma, \\ a_2 &= a_{-2}=\frac{1}{\sqrt{2}}\beta\sin\gamma, \end{aligned} \tag{3}$$

where β represents the total deformation with

$$\sum_{\nu}|a_\nu|^2=\beta^2, \tag{4}$$

and γ represents the degree of triaxiality.

The deviation of $R(\theta,\phi)$ from R_0 is given by

$$\begin{aligned} \Delta R(\theta,\phi) &= R(\theta,\phi)-R_0 \\ &= \sqrt{\frac{5}{16\pi}}R_0\beta[\cos\gamma(3\cos^2\theta-1) \\ &\quad +\sqrt{3}\sin\gamma\sin^2\theta\cos2\phi]. \end{aligned} \tag{5}$$

It can be proven that all quadrupole-deformed shapes can be covered by γ within $[0,\frac{\pi}{3}]$. Thus the deviations of $R(\theta,\phi)$ from R_0 along the principal axes

$$\begin{aligned} \Delta R_1 &= R_1-R_0=R\left(\frac{\pi}{2},0\right)-R_0, \\ \Delta R_2 &= R_2-R_0=R\left(\frac{\pi}{2},\frac{\pi}{2}\right)-R_0, \\ \Delta R_3 &= R_3-R_0=R(0,\phi)-R_0, \end{aligned} \tag{6}$$

can be summarized as

$$\Delta R_\lambda=\sqrt{\frac{5}{4\pi}}R_0\beta\cos\left(\gamma-\frac{2\lambda\pi}{3}\right) \quad \text{with} \quad \lambda=1,\ 2,\ 3. \tag{7}$$

Specifically, one may find

$$\Delta R_1=\Delta R_2=-\sqrt{\frac{5}{16\pi}}R_0\beta, \ \ \Delta R_3=\sqrt{\frac{5}{4\pi}}R_0\beta, \tag{8}$$

at $\gamma=0$;

$$\Delta R_1=\Delta R_3=\sqrt{\frac{5}{16\pi}}R_0\beta, \ \ \Delta R_2=-\sqrt{\frac{5}{4\pi}}R_0\beta, \tag{9}$$

at $\gamma=\frac{\pi}{3}$;

$$\Delta R_1=0, \ \ \Delta R_2=-\Delta R_3=-\sqrt{\frac{15}{16\pi}}R_0\beta, \tag{10}$$

at $\gamma=\frac{\pi}{6}$. If only $\beta>0$ is allowed, the above results indicate that $\gamma=0$ represents the prolate shape, $\gamma=\frac{\pi}{3}$ represents the oblate shape, and $\gamma=\frac{\pi}{6}$ corresponds to the most triaxial shape.

Although the deformation parameters β and γ are not observables, one can judge the geometrical shape of a deformed nucleus from its rotational spectrum if and only if the nucleus is assumed to be rigid. The rotor Hamiltonian is given by [4, 14]

$$H_{\rm rot}=\frac{1}{2\Im_1}L_1^2+\frac{1}{2\Im_2}L_2^2+\frac{1}{2\Im_3}L_3^2, \tag{11}$$

where L_α is the projection of the angular momentum along the α-th body-fixed principal axis and $\Im_\alpha$ is the corresponding moment of inertia. In the following, only rigid or irrotational ellipsoids are assumed to discuss the β- and γ-dependence of the moments of inertia.

For a rigid ellipsoid with uniform mass density distribution, the moments of inertia along the principal axes may be expressed as

$$\begin{aligned} \Im_1 &= \Gamma_1=\frac{M}{5}(R_2^2+R_3^2), \\ \Im_2 &= \Gamma_2=\frac{M}{5}(R_1^2+R_3^2), \\ \Im_3 &= \Gamma_3=\frac{M}{5}(R_1^2+R_2^2), \end{aligned} \tag{12}$$

where M is the mass of the ellipsoid. Substituting R_i with $i=1,\ 2,\ 3$ given by Eq. (6) into (12), one has

$$\begin{aligned} \Gamma_1 &= 2C\left[1+D\cos\left(\gamma+\frac{\pi}{3}\right)+D^2\left(\frac{1}{4}\cos\left(2\gamma-\frac{\pi}{3}\right)+\frac{1}{2}\right)\right], \\ \Gamma_2 &= 2C\left[1+D\cos\left(\gamma-\frac{\pi}{3}\right)+D^2\left(\frac{1}{4}\cos\left(2\gamma+\frac{\pi}{3}\right)+\frac{1}{2}\right)\right], \\ \Gamma_3 &= 2C\left[1+D\cos(\gamma-\pi)+D^2\left(\frac{1}{4}\cos(2\gamma+\pi)+\frac{1}{2}\right)\right], \end{aligned} \tag{13}$$

where $C=\frac{MR_0^2}{5}$ and $D=\sqrt{\frac{5\beta^2}{4\pi}}$, which can be further simplified as

$$\Gamma_\lambda=2C\left[1-D\cos\left(\gamma-\frac{2\lambda\pi}{3}\right)-\frac{D^2}{2}\cos^2\left(\gamma+\frac{\lambda\pi}{3}\right)+\frac{3D^2}{4}\right] \tag{14}$$

with $\lambda=1,\ 2,\ 3$.

It can easily be found that $\Gamma_1=\Gamma_2>\Gamma_3$ at $\gamma=0$ corresponds to the prolate shape, $\Gamma_1=\Gamma_3<\Gamma_2$ at $\gamma=\frac{\pi}{3}$ corresponds to the oblate shape, and $\Gamma_2>\Gamma_1>\Gamma_3$ at $\gamma=\frac{\pi}{6}$ corresponds to the most triaxial shape. It is obvious that the dynamical shape characterized by the moments of inertia $\frac{1}{2\Im_\alpha}$ with $\alpha=1,\ 2,\ 3$ is always consistent with the geometric shape characterized by the Bohr variable γ for the rigid type ellipsoid. Moreover, when $\Gamma_1=\Gamma_2$ or $\Gamma_1=\Gamma_3$, the spectrum of (11) obeys the rotational $L(L+1)$-law within each rotational band. Therefore, the spectrum of the prolate or the oblate rigid ellipsoid is called regular.

On the other hand, for an irrotational ellipsoid with the same mass density distribution, one may write the moments of inertia along the principal axes as [5]

$$\begin{aligned} \Im_1 &= \Gamma_1'=\frac{M}{5}\frac{(R_2^2-R_3^2)^2}{R_2^2+R_3^2}, \\ \Im_2 &= \Gamma_2'=\frac{M}{5}\frac{(R_1^2-R_3^2)^2}{R_1^2+R_3^2}, \\ \Im_3 &= \Gamma_3'=\frac{M}{5}\frac{(R_1^2-R_2^2)^2}{R_1^2+R_2^2}. \end{aligned} \tag{15}$$

Specifically, the moments of inertia of the irrotational ellipsoid shown in (15) may be expressed as functions of β and γ according to Eq. (6) as

$$\begin{aligned}
\Gamma_1' &= \frac{C\left[2\sqrt{3}D\sin\left(\gamma-\frac{2\pi}{3}\right)-\frac{\sqrt{3}D^2}{2}\sin\left(2\gamma+\frac{2\pi}{3}\right)\right]^2}{2+D^2-2D\cos\left(\gamma-\frac{2\pi}{3}\right)-\frac{D^2}{2}\cos\left(2\gamma+\frac{2\pi}{3}\right)},\\
\Gamma_2' &= \frac{C\left[2\sqrt{3}D\sin\left(\gamma-\frac{4\pi}{3}\right)-\frac{\sqrt{3}D^2}{2}\sin\left(2\gamma+\frac{4\pi}{3}\right)\right]^2}{2+D^2-2D\cos\left(\gamma-\frac{4\pi}{3}\right)-\frac{D^2}{2}\cos\left(2\gamma+\frac{4\pi}{3}\right)},\\
\Gamma_3' &= \frac{C\left[2\sqrt{3}D\sin\gamma-\frac{\sqrt{3}D^2}{2}\sin2\gamma\right]^2}{2+D^2-2D\cos\gamma-\frac{D^2}{2}\cos2\gamma},
\end{aligned} \tag{16}$$

which may be rewritten uniformly as

$$\Gamma_\lambda'=\frac{C\left[2\sqrt{3}D\sin\left(\gamma-\frac{2\lambda\pi}{3}\right)-\frac{\sqrt{3}D^2}{2}\sin\left(2\gamma+\frac{2\lambda\pi}{3}\right)\right]^2}{2+D^2-2D\cos\left(\gamma-\frac{2\lambda\pi}{3}\right)-\frac{D^2}{2}\cos\left(2\gamma+\frac{2\lambda\pi}{3}\right)}, \tag{17}$$

for λ=1, 2, 3. Since D or β is usually a small quantity, to the leading order of D, the moments of inertia of the irrotational ellipsoid are given by

$$\Gamma_\lambda'=6CD^2\sin^2\left(\gamma-\frac{2\lambda\pi}{3}\right). \tag{18}$$

By submitting the collective mass parameter defined as $B=\frac{3}{8\pi}MR_0^2$, one may get the familiar form with [6]

$$\Gamma_\lambda'=4B\beta^2\sin^2\left(\gamma-\frac{2\lambda\pi}{3}\right), \tag{19}$$

which can also be obtained from the derivation shown in Refs. [5, 6] by using the quantization procedure.

According to (19), in comparison to the rigid type shown in (14), $\Gamma_1'=\Gamma_2'=3B\beta^2$ and $\Gamma_3'=0$ in the prolate case at γ=0, $\Gamma_1'=\Gamma_3'=3B\beta^2$ and $\Gamma_2'=0$ in the oblate case at $\gamma=\frac{\pi}{3}$, and $\Gamma_2'=\Gamma_3'=B\beta^2$ and $\Gamma_1'=4B\beta^2$ in the most triaxial case at $\gamma=\frac{\pi}{6}$. It should be noted that the moments of inertia of the irrotational type ellipsoid at $\gamma=\pi/6$ is symmetric with respect to the 2nd and 3rd principal axes exchange though the geometric shape is most triaxial according to (10). It is clear that the dynamical shape characterized by the moments of inertia $\frac{1}{2\Im_\alpha}$ is inconsistent with the geometric shape characterized by the Bohr variable γ for the irrotational type ellipsoid in either the oblate case or the most triaxial case.

3 Comparison of the rigid and irrotational ellipsoid dynamics

The quantum dynamics of a rotor described by (11) is determined by relative magnitudes of the moments of inertia. As a consequence, differences and similarities in the spectral patterns and E2 transitional characteristics of the rigid ellipsoid and those of the irrotational ellipsoid can be analyzed accordingly.

It should be noted that, no matter whether a quantum ellipsoid with exact axial-symmetry is rigid or irrotational, its arbitrary rotation around its axial-symmetry axis is quantum mechanically undetectable due to the additional $O(2)$ symmetry. In this extreme case, its spectrum involves only the K=0 band as clarified in Ref. [6], of which the levels obey the $L(L+1)$-law, where L and K is the total angular momentum and its projection onto the symmetric principal axis.

As shown in the previous section, the axially-symmetric situations occur at γ=0 and $\pi/3$ corresponding to the prolate and oblate shape, respectively, for the rigid type and at $\gamma=0$, $\pi/6$, and $\pi/3$ for the irrotational type. As a result, one cannot tell whether the ellipsoid is rigid or irrotational from its spectrum when $\gamma=0$ or $\gamma=\pi/3$. Although the axial-symmetric situation is unrealistic in describing the rotational motion of deformed nuclei, a comparison of spectral characteristics of the rigid ellipsoid with those of the irrotational one in this extreme case is instructive. Actually, up to some scaling factor, the spectra of the two types of ellipsoid are the same at γ=0 because the relation $\Im_1=\Im_2>\Im_3$ is satisfied for both types. Moreover, there is no distinction of the irrotational ellipsoid at γ=0 from that at $\gamma=\pi/3$ in the spectra because the energy levels generated from the two are the same. In contrast, the scaling of excitation energies of the prolate ellipsoid is different from that of the oblate one in the rigid case as shown from the moments of inertia given in (14). An interesting point is that, up to some scaling factor, the spectrum of the irrotational ellipsoid in the most triaxial case at $\gamma=\pi/6$ coincides with that of the rigid one in the oblate case at $\gamma=\pi/3$. Therefore, the spectral characteristics of ellipsoids of different type but of different geometric shape may be quite similar, even when the axial symmetry is slightly broken.

In fact, if only the leading order of D is considered, the moments of inertia for the rigid case shown in (14) may be expressed as

$$\Gamma_\lambda=2C\left[1-D\cos\left(\gamma-\frac{2\lambda\pi}{3}\right)\right], \tag{20}$$

since $D=\sqrt{\frac{5\beta^2}{4\pi}}$ is generally a small quantity with $0<D\ll1$, while the moments of inertia for irrotational

case shown in (18) can be rewritten as

$$\Gamma'_\lambda = 3CD^2\left[1-\cos\left(2\gamma-\frac{4\lambda\pi}{3}\right)\right]. \tag{21}$$

Comparing (20) with (21), it is obvious that, up to some scaling factor, there is a one-to-one correspondence between the moments of inertia of the rigid type shown in (20) at $\gamma=2t$ with $0\leqslant t\leqslant\pi/6$ and those of the irrotational type shown in (21) with the 1st and the 2nd principal axis exchange at $\gamma=t$, even for $D\ll 1$.

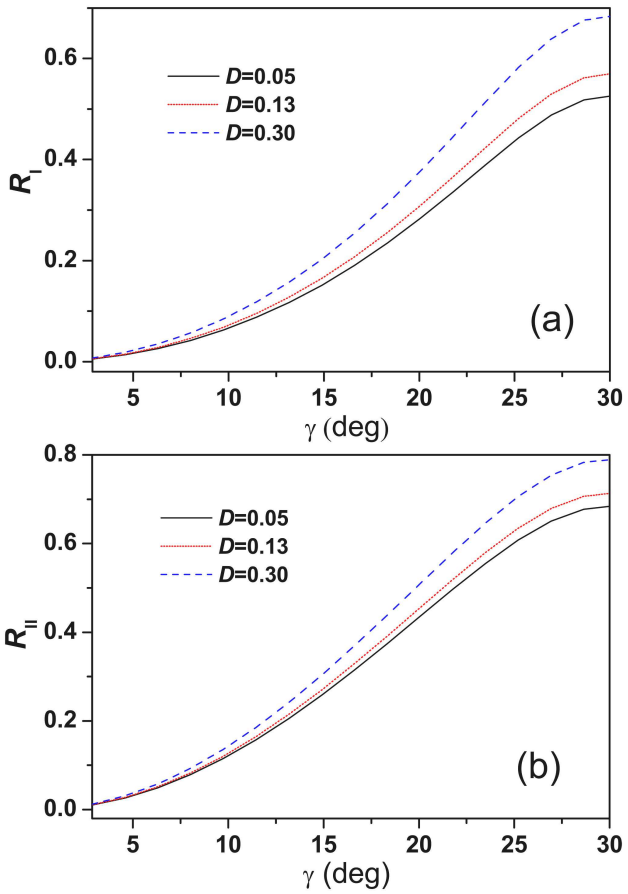

Fig. 1. (color online) The quantities $R_{\rm I}$ and $R_{\rm II}$ with $D=0.05$, 0.13, 0.30 are shown as functions of γ (in degree).

Furthermore, it can be shown that relative magnitudes of the moments of inertia given by (20) at $\gamma=\pi/6$ are similar to those shown in (21) at $\gamma=\pi/12$ since the relations $\Im_a>\Im_b>\Im_c$ and $(\Im_a+\Im_c)/2=\Im_b$ are satisfied for both cases with any given D value, where $(a,\ b,\ c)$ represents (1, 2, 3) for the rigid case and (2, 1, 3) for the irrotational case. To illustrate the effect of D (or β) on the level structure, we take two typical energy ratios, $E_{2_2^+}/E_{2_1^+}$ and $E_{3_1^+}/E_{2_1^+}$, as examples. Explicitly, the two energy ratios can be analytically expressed as

$$R_{\rm irroI} \equiv \frac{E_{2_2^+}}{E_{2_1^+}}=\frac{3+\sqrt{5+4\cos(6\gamma)}}{3-\sqrt{5+4\cos(6\gamma)}}, \tag{22}$$

$$R_{\rm irroII} \equiv \frac{E_{3_1^+}}{E_{2_1^+}}=\frac{6}{3-\sqrt{5+4\cos(6\gamma)}}, \tag{23}$$

for those solved from the irrotational type rotor and

$$R_{\rm rigI} \equiv \frac{E_{2_2^+}}{E_{2_1^+}}=\frac{4-D^2+\sqrt{D^2(4+D^2+4D\cos(3\gamma))}}{4-D^2-\sqrt{D^2(4+D^2+4D\cos(3\gamma))}}, \tag{24}$$

$$R_{\rm rigII} \equiv \frac{E_{3_1^+}}{E_{2_1^+}}=\frac{2(4-D^2)}{4-D^2-\sqrt{D^2(4+D^2+4D\cos(3\gamma))}} \tag{25}$$

for those solved from the rigid type rotor. It is clear that the energy ratios in the irrotational case depend on only the γ variable but the ratios in the rigid case depend on both the γ and β variables. Further, one can define the quantities $R_{\rm I}$ and $R_{\rm II}$ as $R_{\rm I}(\gamma)=R_{\rm rigI}(\gamma)/R_{\rm irroI}(\gamma)$ and $R_{\rm II}(\gamma)=R_{\rm rigII}(\gamma)/R_{\rm irroII}(\gamma)$ to test the D dependence of the difference between the two types of rotor, with the calculated results given in Fig. 1. As clearly seen from Fig. 1, the values of both $R_{\rm I}$ and $R_{\rm II}$ increase monotonically as γ and D increase, which indicates that the difference in energy ratios between the two types of model defined above may become small for large β and γ deformations.

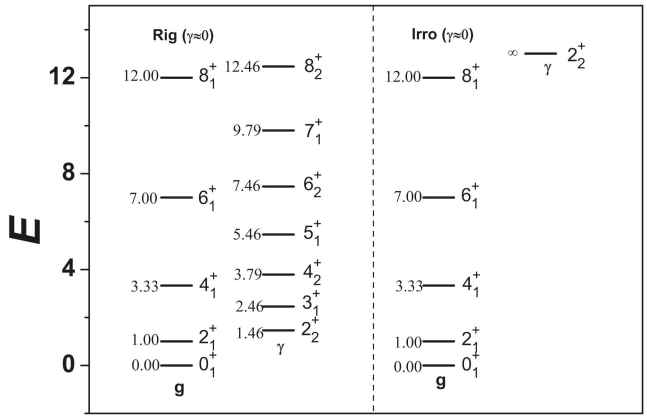

Fig. 2. Some low-lying levels in the ground- and γ-band of the prolate case for the rigid (rig) ellipsoid (left) and the irrotational (irro) one (right), in which L_ξ^+ denotes the ξ-th positive-parity state with the angular momentum quantum number L, and all the energy values have been normalized to the first 2^+ energy in the ground band.

A further comparison between the two types of ellipsoid should be made for both level patterns and E2 transitional characteristics. To obtain the energy levels and E2 transitional rates, numerical diagonalization of

the Hamiltonian (11) should be carried out. Eigenfunctions Ψ^K_{LM} of the general rotor Hamiltonian (11) may be expanded in terms of the Wigner D-functions with

$$\Psi^{\xi}_{LM}=\sum_K C^{\xi}_K \Psi^K_{LM}, \tag{26}$$

where M is the quantum number of the angular momentum projection onto the third axis in the laboratory frame, $\{C^{\xi}_K\}$ are the expansion coefficients, ξ is an additional quantum number needed to label different eigenstates with the same quantum number L and M, and

$$\Psi^K_{LM} = \sqrt{\frac{2L+1}{16\pi^2(1+\delta_{K0})}}[D^{(L)*}_{M,K}(\theta_1,\theta_2,\theta_3) +(-1)^L D^{(L)*}_{M,-K}(\theta_1,\theta_2,\theta_3)], \tag{27}$$

in which $D^{(L)}_{M,K}(\theta_1,\ \theta_2,\ \theta_3)$ is the Wigner D-function of Euler angles θ_1, θ_2, and θ_3. The Hamiltonian (11) under the basis spanned by (27) is block-diagonalized. The block-diagonalized result is due to the invariance of (11) under rotations by π around the principal axes [9]. These rotations, which can be written as $T_\alpha=\mathrm{e}^{-\mathrm{i}\pi L_\alpha}$ with $\alpha=1$, 2, and 3, together with the identity operation, generate the Vieregruppe (D_2) group. The invariance means that $[H_{\rm rot},\ T_\alpha]=0$ for $\alpha=1$, 2, and 3. Generally, wavefunctions that carry the irreps of the D_2 can be constructed by a combination of Wigner D-functions with

$$\Psi^{\lambda\mu K}_{LM} = \sqrt{\frac{2L+1}{16\pi^2(1+\delta_{K0})}}[D^{(L)*}_{M,K}(\theta_1,\theta_2,\theta_3) +(-1)^{\lambda+\mu+L} D^{(L)*}_{M,-K}(\theta_1,\theta_2,\theta_3)], \tag{28}$$

where λ and μ are integers. The D_2 group has four representations denoted as A, B_1, B_2, and B_3, respectively, in which only the A-type representation is allowed for even–even nuclei [9]. In the A-type case, both λ and μ should be taken as even integers, by which (28) is reduced to (27) with $K=0$ or $K=$ even, in which only positive K values need to be considered. The multiplicity of L is given as $(L+2)/2$ for $L=$even and $(L-1)/2$ for $L=$odd. As shown in [8], the allowed L and K are $L=0$, 2, 4, 6, $\cdots$, for $K=0$ and $L=K$, $K+1$, $K+2$, $K+3$, $\cdots$, for $K=$even.

The D_2 symmetry holds for both the asymmetric and the symmetric cases of (11). In the dynamically axially-symmetric cases, however, in addition to the D_2 symmetry, there is the additional $O(2)$ symmetry. The $O(2)$ group consists of rotations around the symmetric principal axis. When $\Im_1=\Im_2\neq\Im_3$ for example, the eigenfunctions of (11) in this case are those shown in (27). However, (11) in this case should also be invariant under arbitrary rotation round the 3rd principal axis, namely, $[H_{\rm rot},\ \mathrm{e}^{-\mathrm{i}\phi L_3}]=0$ for arbitrary $\phi\in[0,2\pi]$. The additional $O(2)$ symmetry requires that only $K=0$ is allowed, because the eigenfunctions given by (27) under the $O(2)$ rotation transforms as

$$\mathrm{e}^{-\mathrm{i}\phi L_3}\Psi^K_{L,M} = \sqrt{\frac{2L+1}{16\pi^2(1+\delta_{K0})}}[\mathrm{e}^{-\mathrm{i}\phi K} D^{(L)*}_{M,K}(\theta_1,\theta_2,\theta_3) +(-1)^L \mathrm{e}^{\mathrm{i}\phi K} D^{(L)*}_{M,-K}(\theta_1,\theta_2,\theta_3)], \tag{29}$$

which is invariant only when $K=0$. The additional $O(2)$ symmetry explains why only the ground band with $K=0$ emerges for the axially-symmetric rotor Hamiltonian [6]. Actually, the axially-symmetric rotor Hamiltonian in this case is invariant under the $O(2)\overline{\bigotimes}D_2$ transformation, where $\overline{\bigotimes}$ stands for the semi-direct product.

As discussed above, there is a one-to-one correspondence between the moments of inertia of the rigid type at $\gamma=2t$ and those of the irrotational type at $\gamma=t$, so it would be interesting to give a close comparison between the two types of rotor under such situations. Specifically, we compare the rotational features of an ellipsoid of the rigid type with that of the irrotational type at several special γ points, of which situations with exact axial-symmetry are avoided because the exact axial-symmetry is unrealistic in describing deformed nuclei. In order to avoid exact axial-symmetry, a very small quantity ε is always assumed to be added to the γ values corresponding to the exact axially-symmetric cases, though the results calculated with $\gamma+\varepsilon$ and those with γ are approximately taken as the same. Moreover, besides the ground band, other bands in this case also show up with the near axial-symmetry assumption.

Table 1. Some typical B(E2) values for the two types of ellipsoid in the prolate case corresponding to the case shown in Fig. 2, where all transitions are normalized to $B(\mathrm{E2};2_\mathrm{g}\to0_\mathrm{g})$, of which L_g and L_γ denote the states with angular momentum quantum number L in the ground band and those in the γ-band, respectively. In the calculations, the γ value in the quadrupole operator (31) has been taken the same as that used in the corresponding moments of inertia.

$L_\mathrm{i}\to L_\mathrm{f}$	rig	irro	$L_\mathrm{i}\to L_\mathrm{f}$	rig	irro
$2_\mathrm{g}\to0_\mathrm{g}$	100	100	$2_\gamma\to0_\mathrm{g}$	0	–
$4_\mathrm{g}\to2_\mathrm{g}$	143	143	$2_\gamma\to2_\mathrm{g}$	0	–
$6_\mathrm{g}\to4_\mathrm{g}$	157	157	$3_\gamma\to2_\gamma$	179	–
$8_\mathrm{g}\to6_\mathrm{g}$	165	165	$4_\gamma\to3_\gamma$	133	–

Some low-lying levels in both the ground band and the γ-band of the rigid ellipsoid at $\gamma=2t$ and those of the irrotational ellipsoid at $\gamma=t$ with $t\approx0$, $t=\pi/12$, and $t\approx\pi/6$ are shown in Figs. 2–4, respectively, where $\beta=0.5$ is set for all these cases. B(E2) values of the above cases for both the intra- and inter-band transitions are calculated according to

$$B(\mathrm{E2};L_\mathrm{i}\to L_\mathrm{f})=\frac{|\langle L_\mathrm{f}\|\hat{Q}\|L_\mathrm{i}\rangle|^2}{2L_\mathrm{i}+1}, \tag{30}$$

where the quadrupole operator is given as [5, 6]

$$\hat{Q}_u=\frac{3Ze}{4\pi}R_0^2\,\beta[\cos(\gamma)D^{(2)}_{u,0}+\frac{1}{\sqrt{2}}\sin(\gamma)(D^{(2)}_{u,2}+D^{(2)}_{u,-2})], \quad (31)$$

in which e is assumed to be the effective charge. Unless specified separately, the β and γ values in (31) are taken to be the same as those in the moments of inertia for a given type of ellipsoid. Some typical B(E2) values of both the intra- and inter-band transitions of the rigid ellipsoid at $\gamma=2t$ and those of the irrotational ellipsoid at $\gamma=t$ for $t\approx 0$, $t=\pi/12$, and $t\approx\pi/6$ are shown in Tables 1–3, respectively.

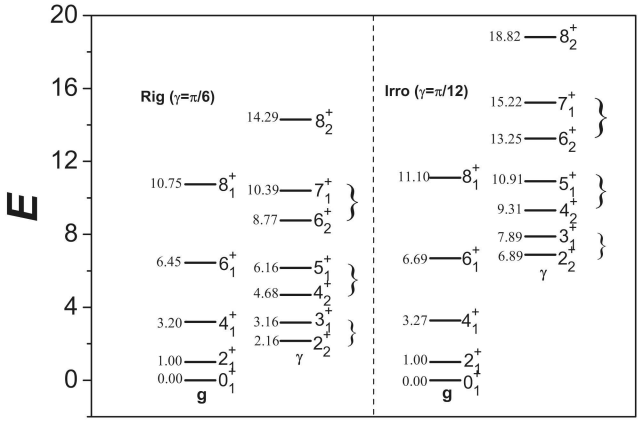

Fig. 3. The low-lying levels in the ground- and γ-band of the triaxial case at $t=\pi/12$ for the rigid (rig) ellipsoid (left) and the irrotational (irro) one (right), where all the levels are normalized to the 2^+_1 energy in each case.

Table 2. Some typical B(E2) values for the two types of ellipsoid in the triaxial case corresponding to the case shown in Fig. 3, where all transitions are normalized to $B(\mathrm{E2};2_\mathrm{g}\to 0_\mathrm{g})$. In the calculations, the γ value in the quadrupole operator (31) has been taken the same as that used in the corresponding moments of inertia.

$L_\mathrm{i}\to L_\mathrm{f}$	rig	irro	$L_\mathrm{i}\to L_\mathrm{f}$	rig	irro
$2_\mathrm{g}\to 0_\mathrm{g}$	100	100	$2_\gamma\to 0_\mathrm{g}$	73	6
$4_\mathrm{g}\to 2_\mathrm{g}$	98	145	$2_\gamma\to 2_\mathrm{g}$	6	15
$6_\mathrm{g}\to 4_\mathrm{g}$	99	165	$3_\gamma\to 2_\gamma$	179	179
$8_\mathrm{g}\to 6_\mathrm{g}$	101	179	$4_\gamma\to 3_\gamma$	207	123

As shown in Fig. 2, both the ground band and the γ-band for the two types of ellipsoids of the prolate shape follow the $L(L+1)$-law exactly except that the band head energy of the γ-band is infinite in the irrotational case due to $\Gamma_3'=0$ at $\gamma\approx 0$. Notably, $E_{4_\mathrm{g}}/E_{2_\mathrm{g}}=3.33$ is the direct evidence that the levels in the ground band obey the $L(L+1)$-law. For the γ-band, it is convenient to use the ratio defined as $R_\gamma=\frac{E_{4_\gamma}-E_{2_\gamma}}{E_{3_\gamma}-E_{2_\gamma}}$, of which the ratio $R_\gamma=2.33$ if the $L(L+1)$-law is satisfied. It should be noted that levels in the ground band and those in the γ-band in the prolate case are grouped by those with $K^\pi=0^+$ and those with $K^\pi=2^+$, respectively, where K is the projection of angular momentum onto the 3rd principal axis. In this case, the Hamiltonian is nearly axially-symmetric [5] because $\Im_1\approx\Im_2>\Im_3$ is always satisfied for both the rigid and irrotational type when $\gamma\approx 0$. Furthermore, the normalized results given in Table 1 show that the allowed transitional rates for the two types of ellipsoid in the prolate case are also the same, while the inter-band transitions for the irrotational type are prohibited.

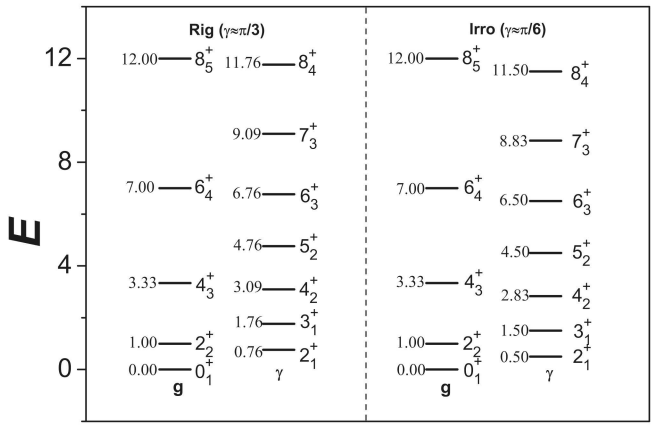

Fig. 4. The low-lying levels in the ground- and γ-band of the $t\approx\pi/6$ case for the rigid (rig) ellipsoid (left) and the irrotational (irro) one (right), where all the levels are normalized to the 2^+_2 energy in each case.

For the triaxial case, the results calculated for the rigid type at $\gamma=\pi/6$ and the corresponding results calculated for the irrotational type at $\gamma=\pi/12$ are given in Fig. 3 and Table 2. It can be seen from Fig. 3 that the level patterns for the rigid type are quite similar to those for the irrotational type except that the γ-band head energy is relatively high. Particularly, the odd–even staggering, which is regarded as a signature of a triaxial rotor [11, 19], appears in the γ-band of both types of ellipsoid as indicated by braces in Fig. 3. In addition, $R_\gamma=2.52$ for the rigid type and $R_\gamma=2.42$ for the irrotational type, which indicates that levels in the γ-band of the two types of ellipsoid deviate noticeably from the $L(L+1)$-law. On the other hand, the E2 transitional rates given in Table 2 show that the $B(\mathrm{E2},\ L+2\to L)$ value of intra-band transition in the ground band gradually changes slightly with the increasing of L for the rigid case, but increases noticeably with the increasing of L for the irrotational case.

The results calculated for the rigid type at $\gamma\approx\pi/3$ and the corresponding results for the irrotational type at $\gamma\approx\pi/6$ are shown in Fig. 4 and Table 3. It is clearly

shown in Fig. 4 that the levels in the ground band of both the rigid and irrotational type ellipsoid follow the $L(L+1)$-law exactly. Since $R_\gamma=2.33$ for both types, the levels in the γ-band of both types of ellipsoid also follow the $L(L+1)$-law exactly. A notable feature of both types is that the levels with L even in the γ-band are all lower in energy than the corresponding ones in the ground band as shown in Fig. 4. It should be emphasized that the Hamiltonian (11) in this case is nearly axially-symmetric because $\Gamma_1\approx\Gamma_3<\Gamma_2$ for the rigid type and $\Gamma'_2\approx\Gamma'_3<\Gamma'_1$ for the irrotational type. As a consequence, the levels with $\eta=0$ and those with $\eta=2$ for the rigid case are taken to be in the ground band and in the γ-band respectively, where η is the projection of angular momentum onto the 2nd principal axis. For the irrotational type, the levels with $\alpha=0$ and those with $\alpha=2$ are taken to be in the ground band and in the γ-band respectively, where α is the projection of angular momentum onto the 1st principal axis because the 1st principal axis is the symmetric axis in this case. Thus, it is easy to understand why the levels in each band shown in Fig. 4 all follow the $L(L+1)$-law exactly. In contrast to the prolate case shown in Table 1, in which B(E2) values of the intra-band transitions within the ground band for both rigid and irrotational type are the same, the E2 transitional characteristics of the rigid and irrotational type shown in Table 3 are completely different. It is clearly shown for the rigid type case that the inter-band transitions between the ground- and γ-bands are completely prohibited, but the intra-band transitions are allowed and noticeable, while the situation in the irrotational type case is completely the inverse, in which the intra-band transitions in each band are nearly prohibited, but the inter-band transitions between two bands are allowed and noticeable.

Table 3. Some typical B(E2) values for the two types of ellipsoid in the $t\approx\pi/6$ case corresponding to those shown in Fig. 4, where all transitions are normalized to $B(\mathrm{E2};2_\mathrm{g}\to0_\mathrm{g})$. In the calculations, the γ value in the quadrupole operator (31) has been taken the same as that used in the corresponding moments of inertia.

$L_\mathrm{i}\to L_\mathrm{f}$	rig	irro	$L_\mathrm{i}\to L_\mathrm{f}$	rig	irro
$2_\mathrm{g}\to0_\mathrm{g}$	100	0	$2_\gamma\to0_\mathrm{g}$	0	100
$4_\mathrm{g}\to2_\mathrm{g}$	143	1	$2_\mathrm{g}\to2_\gamma$	0	143
$6_\mathrm{g}\to4_\mathrm{g}$	157	4	$3_\gamma\to2_\gamma$	179	0
$8_\mathrm{g}\to6_\mathrm{g}$	165	6	$4_\gamma\to3_\gamma$	133	1

Table 4. Some typical B(E2) values for the two types of ellipsoid corresponding to the case shown in Fig. 5, where all transitions are normalized to $B(\mathrm{E2};2_{g_1}\to0_{g_1})$. In the calculations, the γ value in the quadrupole operator (31) has been taken the same as that used in the corresponding moments of inertia.

$L_\mathrm{i}\to L_\mathrm{f}$	rig	irro	$L_\mathrm{i}\to L_\mathrm{f}$	rig	irro
$2_{\mathrm{g}_1}\to0_{\mathrm{g}_1}$	0	100	$2_{\gamma_1}\to0_{\mathrm{g}_1}$	100	0
$4_{\mathrm{g}_1}\to2_{\mathrm{g}_1}$	0	141	$2_{\gamma_1}\to2_{\mathrm{g}_1}$	0	143
$6_{\mathrm{g}_1}\to4_{\mathrm{g}_1}$	0	173	$3_{\gamma_1}\to2_{\gamma_1}$	0	179
$8_{\mathrm{g}_1}\to6_{\mathrm{g}_1}$	0	191	$4_{\gamma_1}\to3_{\gamma_1}$	133	1

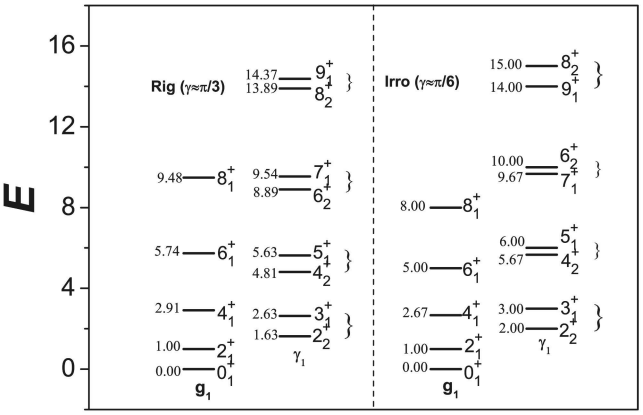

Fig. 5. The low-lying levels in the ground- and γ-band of the $t\approx\pi/6$ case for the rigid (rig) ellipsoid (left) and the irrotational (irro) one (right), where the ground- and the γ-bands are reassigned according to the energy value of the levels with the same L shown in the text and labeled by g_1 and γ_1 respectively. All the levels are normalized to the 2^+_1 energy in each case.

Although the Hamiltonian for the irrotational type case at $\gamma=t=\pi/6$ is nearly axially-symmetric just as that for the rigid type case at $\gamma\approx\pi/3$ corresponding to the oblate shape, the irrotational type at $\gamma\approx\pi/6$ is often referred to as being triaxial [5, 19] because the corresponding geometrical shape is indeed most triaxial at $\gamma=\pi/6$. Actually, the levels shown in Fig. 4 can also be regrouped into a new ground- and a new γ-band according to the energy value of the levels with the same L. Specifically, the new ground band consists of the lowest levels with $L=0$ or even, while the new γ-band consist of the next-to-lowest levels with $L=$even or the lowest ones with $L=$odd, which is shown in Fig. 5. One can observe that the level pattern shown in Fig. 4 and that shown in Fig. 5 are quite different. The odd–even staggering appears in the new γ-band for both types of ellipsoid, and the level ordering in the γ-band for the irrotational type case is even reversed, which are all considered to be signals of triaxiality [11, 19]. For E2 transitions, it is shown in Table 4 that the intra-band transitions in both the new ground- and the new γ-band are almost prohibited for the rigid type case. In contrast, the intra-band transition rates in the ground band for the irrotational case present a monotonic increasing with the increasing

of L, as shown in Table 4. Hence, it is recognized that the triaxiality shown in Fig. 5 emerges from the rearrangement of the levels of the oblate spectrum of the irrotational type case shown in Fig. 4, which results in a different band assignment.

4 Summary

In summary, we have presented a detailed comparison of dynamical shape characterized by the moments of inertia of the rigid type ellipsoid to that characterized by those of the irrotational type. It is shown that, up to some energy scaling factor, the level patterns of the rigid ellipsoid at $\gamma = 2t$ are similar to those of the irrotational type at $\gamma = t$ to the leading order of the deformation parameter. Numerical investigation of the excitation energies and B(E2) values for the two types of the model was also carried out, in which the triaxial situations were particularly emphasized. It was shown in Fig. 2, Fig. 3 and Table 1, Table 2 that both level patterns and E2 transitional characteristics of the two types of the model with prolate and triaxial geometric shape are quite similar. On the other hand, it was shown in Fig. 4 and Fig. 5 that the level patterns of the rigid type model with $\gamma=\pi/3$ are similar to those of the irrotational type with $\gamma=\pi/6$. However, the E2 transitional characteristics of the types of rotor are quite different in such cases as seen in Table 3 and Table 4. In addition, the results also indicate that the excited levels in the rigid type model with $\gamma=\pi/3$ and the irrotational type model with $\gamma = \pi/6$ may be regrouped into new ground- and γ-bands, with which the spectrum looks quite similar to that of a triaxial rotor. As a result, a similar rotational spectrum may be generated from different types of model with different γ deformation parameters. Based on the low-lying levels observed in most deformed nuclei, the band assignment shown in Fig. 5 seems more realistic than that shown in Fig. 4, namely the γ-band head energy seems to always be higher than the energy of the first 2^+ state in the ground band.

References

1 R. L. Kronig, and I. I. Rabi, Phys. Rev., **29**: 262–269 (1927)
2 H. B. G. Casimir, *Rotation of a rigid body in quantum mechanics*, (The Hague: Wolters, 1931)
3 A. Bohr, Konggl. Dan. Vid. Selsk. Mat.-fys. Medd., **26**(14): (1952)
4 A. S. Davydov, and G. F. Filippov, Nucl. Phys., **8**: 237–249 (1958)
5 A. Bohr, and B. R. Mottelson, *Nuclear Structure*, (Reading Ma: Benjamin W A Inc., 1975)
6 W. Greiner, and J. A. Maruhn, *Nuclear models*, (Berlin: Springer-Verlag, 1996)
7 H. Ui, Prog. Theor. Phys., **44**: 153–171 (1970)
8 Y. Leschber, and J. P. Draayer, Phys. Lett. B, **190**: 1–6 (1987)
9 O. Castaños, J. P. Draayer, and Y. Z. Leschber, Phys. A, **329**: 33–43 (1998)
10 H. A. Naqvi, C. Bahri, D. Troltenier, J. P. Draayer, A. Z. Faessler, Phys. A, **351**: 259–270 (1995)
11 Yuri F. Smirnov, Nadya A. Smirnova, van Isacker Piet, Phys. Rev. C, **61**: 041302(R) (2000)
12 G. Thiamova, Eur. Phys. J. A, **45**: 81–90 (2010)
13 Y. Zhang, F. Pan, Lian-Rong Dai, and J. P. Draayer, Phys. Rev. C, **90**: 044310 (2014)
14 J. L. Wood, A. M. Oros-Peusquens, R. Zaballa, J. M. Allmond, and W. D. Kulp, Phys. Rev. C, **70**: 024308 (2004)
15 J. M. Allmond, R. Zaballa, A. M. Oros-Peusquens, W. D. Kulp, and J. L. Wood, Phys. Rev. C, **78**: 014302 (2008)
16 J. M. Allmond, J. L. Wood, and W. D. Kulp, Phys. Rev. C, **80**: 021303(R) (2009)
17 J. M. Allmond, J. L. Wood, and W. D. Kulp, Phys. Rev. C, **81**: 051305(R) (2010)
18 Q. B. Chen, S. Q. Zhang, P. W. Zhao, and J. Meng, Phys. Rev. C, **90**: 044306 (2014)
19 N. V. Zamfir, and R. F. Casten, Phys. Lett. B, **260**: 265–270 (1991)